Appl Phys B
DOI 10.1007/s00340-010-4147-y

Applied Physics B
Lasers and Optics

Jet-cooled infrared spectra of molecules and complexes with a cw mode-hop-free external-cavity QCL and a distributed-feedback QCL

X. Liu · Y. Xu · Z. Su · W.S. Tam · I. Leonov

Received: 22 April 2010 / Revised version: 21 June 2010

Abstract The coupling of quantum cascade lasers (QCLs) with an off-axis cavity enhanced absorption (CEA) spectrometer and an astigmatic multiple pass absorption (MPA) spectrometer are described in this paper. A continuous wave (cw) liquid nitrogen cooled distributed-feedback QCL at 5.7 μm and a cw room temperature mode-hop-free external-cavity QCL at 6.1 μm were employed as the light source. For the CEA spectrometer, the effects of mirror size and laser scan rate were evaluated. For the MPA spectrometer, a pair of astigmatic mirrors with a 55 cm mirror distance was aligned to the 366-pass configuration. The jet-cooled samples were generated using a homemade pulsed slit jet nozzle assembly. Two LabVIEW programs were written to automate and synchronize the timing of the laser scan, the pulsed slit jet molecular expansion, and the data acquisition. Infrared spectra of jet-cooled methyl lactate and the Ar–H_2O complex and room temperature N_2O and NH_3 samples were measured using both the rapid scan and the wavelength modulation methods to evaluate the sensitivity and resolution of the CEA and MPA spectrometers. The combination of the MPA spectrometer with the external-cavity QCL using the rapid scan method was found to be the best suited combination to measure high resolution jet-cooled infrared spectra.

X. Liu · Y. Xu (✉) · Z. Su · W.S. Tam · I. Leonov
Department of Chemistry, University of Alberta, Edmonton, Alberta, Canada, T6G 2G2
e-mail: yunjie.xu@ualberta.ca
Fax: +1-780-4928231

Present address:
Z. Su
Chemistry Research Laboratory, Mansfield Road, Oxford University, Oxford, UK, OX1 3TA

1 Introduction

The combination of infrared laser spectroscopy with a molecular jet expansion provides a powerful technique to investigate the structures and dynamics of medium size molecules and clusters. Lead salt diode lasers [1] are one of the most common laser sources used for mid-infrared high resolution molecular spectroscopy. Direct absorption techniques using different types of multi-pass absorption cells [2–4] and continuous wave (cw) cavity ring-down (CRD) technique based on lead salt diode lasers [5] had been developed for molecular spectroscopy. In addition, the narrow line width of a lead salt diode laser provides the foundation to achieve high resolution spectroscopic measurements. CRD spectroscopy has some noticeable shortcomings when used for the jet-cooled spectroscopic measurement. For example, it takes several hours to scan over a 1 cm^{-1} region using the CRD technique in combination with pulsed jet expansions. This is because the laser frequency needs to be stepped narrowly for the high resolution requirement while the repetition rate of a pulsed molecular jet is only a few hertz at best. Cavity enhanced absorption (CEA) spectroscopy is a possible alternative that allows one to take full advantage of both the high reflectivity of ring-down mirror and the rapid scan capability of a diode laser. Unfortunately, the output power of a lead salt diode laser is simply too low for such experiments. In recent years, quantum cascade lasers (QCLs) [6, 7] have attracted much attention as a new type of mid-infrared tunable diode laser because of their superior output power and mode quality when compared to lead salt diode lasers. More recently, significant improvements such as room temperature operation, wide frequency tunability, and narrow line width have been achieved for cw QCL [8]. A number of research groups had successfully applied this new laser technology to trace gas sensing, such as CRD and CEA based detection

Published online: 20 July 2010

of nitric oxide [9–17]. The new improvements with the cw QCLs also make them an attractive light source to carry out high resolution molecular spectroscopy. These new characteristics are particularly important since we are interested in detecting rotationally resolved infrared spectra of medium size organic molecules and complexes, the measurement of which places stringent requirements on the sensitivity and resolution of the infrared spectrometers used. A jet expansion can greatly reduce the spectral congestion and increase the detection sensitivity by transferring almost all the molecular population to the few low lying rotational levels of the ground vibrational state. In particular, a slit nozzle was envisioned for our experiments since it can provide much narrower line width than a pinhole nozzle.

In this report, the design, construction, and performance of a slit jet off-axis CEA spectrometer and the performance of a multiple pass absorption (MPA) spectrometer based on QCLs are described in detail. A cw liquid nitrogen cooled distributed-feedback (DF) QCL at 5.7 μm (Alpes Lasers) and a cw room-temperature mode-hop-free external-cavity (EC) QCL at 6.1 μm (Daylight Solutions) were used as the light sources. In addition, both rapid scan and wavelength modulation spectroscopy (WMS) methods were implemented with both spectrometers. High resolution infrared spectra of the RT static NH_3 and N_2O, and the jet-cooled methyl lactate and the Ar–H_2O complex were measured in order to evaluate the performance of the CEA and the MPA spectrometers. The advantages and disadvantages of these different technical combinations for the measurement of jet-cooled molecular system are discussed.

2 The pulsed slit jet CEA and MPA spectrometers

A schematic diagram of the slit jet off-axis CEA/MPA spectrometer is shown in Fig. 1. The apparatus consists of four main components: (1) the QCL light source; (2) a cavity enhanced absorption (CEA) cell or an astigmatic multi-pass cell as the sample cell; (3) a pulsed slit jet expansion assembly to produce the jet-cooled sample; and (4) the hardware and software for experiment control and data acquisition. In the following, these four main components are described.

2.1 QCL lasers

Two different QCLs were used in the current study. One of them is the DF-QCL that operates from 80 to 110 K with a total frequency coverage from 1760 cm^{-1} (110 K) to 1766 cm^{-1} (80 K). To run this QCL, one needs a liquid nitrogen dewar that can handle the large amount of heat generated by the QCL operation while maintaining a satisfactory temperature stability over a wide temperature range. A specially designed liquid nitrogen laser dewar (Cryo Industries of America, DVT-2090-LMN) with a thermal link

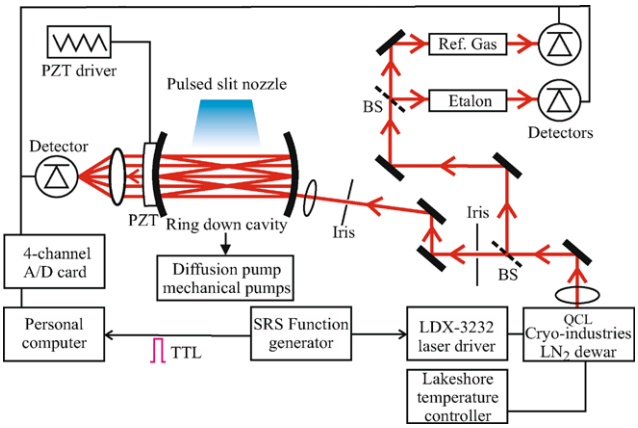

Fig. 1 Schematic diagram of the slit-jet off-axis CEA/MPA spectrometer. The astigmatic multi-pass cell (not shown) used in the MPA spectrometer is situated perpendicular to the CEA cell and points out of the paper plane. Both the DF-QCL (shown) and the EC-QCL (not shown) were used in the experiments

with which one can restrict the liquid nitrogen flow in situ was used. The temperature stability achieved during laser operation was typically better than 0.01 K at a temperature lower than 100 K, and about 0.01∼0.02 K for a higher temperature up to 110 K. In addition, the cold finger was in contact with liquid nitrogen through flexible copper braids and rigidly attached to the bottom frame of the dewar which was directly mounted on a laser table. This improved the laser beam pointing stability compared to the other dewar design where the cold finger was in direct mechanical contact with liquid nitrogen [5]. The QCL diode was installed on a homemade copper laser mount with an additional silicon temperature sensing diode mounted directly underneath to obtain a reliable laser temperature reading. The laser temperature was controlled by a Lakeshore temperature controller (LS340) and its current was provided by a current driver (LDX-3232) from ILX Lightwave Corporation. The current driver was interfaced with a personal computer via a custom LabVIEW experimental control software program. The laser output power was about a few mW on average. An aspheric lens with a focusing length of 11.2 mm was employed to collimate the laser beam. Two irises were inserted into the beam path to remove the unwanted optical fringes by further selecting the central portion of the beam. By placing an infrared camera right before and after the CEA cell, we found that the diameter of the collimated beam was about 2 to 3 mm with a Gaussian like profile.

The second QCL used is the EC-QCL [18, 19] at 6.1 μm, which utilizes a robust, externally tunable laser cavity to generate a broad continuous frequency tuning range from 1592 to 1698 cm^{-1}. The much broader tuning range is one major advantage of the new EC-QCLs when compared with the DF-QCL described above. This new property made them particularly attractive for applications in molecular spec-

troscopy where extensive spectral searches are often required. In addition, the laser is compact, turn-key ready, and user friendly. To ensure the proper operation of the EC-QCL, a water chiller (T255P, ThermoTek) was used to circulate cooling water into the laser case to maintain a temperature of 18.0°C. The finer temperature adjustment was achieved by a built-in thermo-electric cooler and a PID temperature control unit. The laser beam was pre-collimated in factory, with a diameter of ∼1.0 mm and can be ported over 10 m without any noticeable divergence. The whole spectral bandwidth of ∼100 cm^{-1} can be scanned coarsely in a few seconds by a stepper motor which rotates the grating. For high resolution spectroscopic applications, the laser can be finely tuned over ∼1 cm^{-1} by tuning a piezo electric transducer (PZT) attached to the tunable diffraction grating. An external piezo driver (E6-10.00, Polytec PI) was used to drive the laser PZT with a unipolar sine wave with a maximum amplitude of 100 V and a maximum frequency of 100 Hz produced by a function generator (Stanford Research Systems, DS345). Since such tuning is purely mechanical, it was noted in our experiments that the laser frequency shifts slightly from one scan cycle to the next, leading to line broadening (see Sect. 4 for details). Occasionally mechanical jittering of the external-cavity even led to mode-hops. Such effects are particularly severe when laser PZT scan rate goes below 10 Hz and can be substantially minimized with the highest possible laser PZT scan rate, which is 100 Hz at the present time. The EC-QCL frequency can also be varied by current modulation which uses an external sine wave. The modulation depth was estimated to be 0.1 cm^{-1} at 3.0 Vpp (volts-peak-to-peak) amplitude with 50 kHz modulation frequency.

2.2 Sample cells

The sample cells employed in the study are a CEA cell and an astigmatic multi-pass cell. The CEA cell consists of a pair of high reflectivity mirrors ($R \sim 99.98\%$, Los Gatos Research) with 1″ diameter and 1 m radius of curvature (ROC) centered at 5.2 or 6.2 μm. Since the actual CEA experiments were carried out at wavelengths further away from the center wavelengths and the very edges of the mirrors were used, their actual reflectivity values are considerably lower than those specified here. The entrance mirror, whose effective aperture is ∼20 mm in diameter, was attached to a piezoelectric actuator (PiezoMechanik). A pair of kinematic mirror holders, which were secured to a homemade four-rod rigid assembly, provides the tip tilt adjustments for the two ring-down mirrors. This is similar to what was used in the previous CRD experiments with a lead salt diode laser [5]. The mirror separation d is 55 cm, corresponding to a free spectral range of 273 MHz with an on-axis alignment. For the off-axis CEA alignment, the laser beam was designed to make 20 round trips between the ring-down mirrors before tracing itself again. The angle formed by the two radius vectors to the beam spots on the same mirror after one round trip was calculated to be ∼126.5°, based on the equation $\cos\theta = 1 - \frac{d}{\mathrm{ROC}}$. To achieve such a designed alignment, the infrared beam was first brought to coincide with a visible HeNe laser on-axis. The HeNe beam was shifted to trace a standard Herriot cell pattern [20] with the sequential spots separated by about ∼126.5° on each ring-down mirror. It was very difficult to follow the beam path after the first few round trips. We found that it was most efficient to directly optimize the final off-axis alignment by monitoring the infrared detector output on an oscilloscope to achieve the best signal-to-noise ratio (SNR) for a known transition [11, 21]. The typical infrared intensity patterns for the on- and off-axis alignment are shown in Fig. 2. In the on-axis alignment, there are four strong spikes in each mirror PZT period, corresponding to the fundamental TEM_{00} mode, whereas the smaller spikes are due to the higher order modes. In the off-axis alignment, on the other hand, there are many more high order modes excited so that nearly all frequencies were effectively coupled into the cavity and the strong spurious cavity power build-ups were minimized.

For the MPA spectrometer, a homemade astigmatic MPA assembly was used to house a pair of 2″ astigmatic mirrors ($R = 99.2\%$, 3∼10 μm, AMAC-100, Aerodyne Research) and to provide fine tip-tilt and translational adjustments for them. The assembly allows one to pre-align the astigmatic multi-pass mirrors outside the vacuum chamber before installing the whole assembly into the chamber perpendicularly to the CEA cell. The infrared beam entered the central hole of the front mirror and traced out the Lissajous pattern with a rectangular outer boundary, then exited the absorption cell through the same coupling hole. The reentrant condition can be met with a proper combination of mirror separation and rotation angle of the astigmatic axes. Both the 182-pass and 366-pass patterns were located and confirmed by comparing the patterns of the visible laser spots on the mirrors with the simulated pattern map [22]. By adjusting the angle of the entrance beam, we were able to achieve a vertical rectangular outer boundary spot pattern which allows a better overlap of the infrared beam waist with the slit jet. To minimize the condensation of oil vapor onto the mirror surfaces, each mirror is heated to ∼50° by a 120 Ω polyimide heater (Kapton Thermofoil, Minco), which is clamped between a 3 mm thick Teflon heat insulator and a 2.5 mm thick copper heat spreader attached to the backside of the mirror.

In all experiments, an $f = 50$ cm BaF_2 focusing lens was used to couple the laser beam into the sample cell. The infrared beam exiting the sample cell was then focused onto a liquid nitrogen cooled MCT detector (Fermionics Corporation, PV-6-1) with a matching preamplifier (PV MCT-1000).

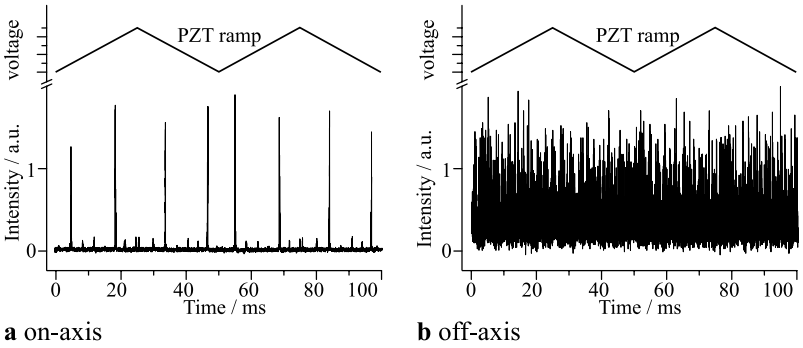

Fig. 2 On-axis and off-axis cavity output pattern from the CEA cell with the DF-QCL: (**a**) on-axis cavity output pattern showing eight bigger spikes and the smaller ones due to the TEM_{00} and higher order transverse modes, respectively; (**b**) off-axis cavity output pattern. Two consecutive piezo ramping periods are given here and the laser frequency was fixed

2.3 Jet expansion

A six way vacuum chamber (Trinos Vacuum Systems Inc.) evacuated by a combination of 8000 L/s oil diffusion pump (Leybold, DIP8000), a roots blower (Leybold, Ruvac WAU251) and a rotary pump (Leybold, Trivac D65B) was used to house both the CEA and MPA assemblies and the pulsed slit jet nozzles. The diffusion pump was equipped with a liquid nitrogen baffle, which helped to minimize the back streaming of the oil vapor in order to protect the highly reflective ring-down mirrors. The jet-cooled molecules and complexes were generated in the jet expansion using the pulsed slit nozzle, which was constructed by modifying a GV series 9 circular nozzle, following the design reported by Maier and co-workers [23]. Briefly, a homemade nozzle cap was constructed to direct the gas pulse exiting the pinhole nozzle through 6 narrow cylindrical channels in a row. The diameters of the channels were 1.0, 1.5 and 2.0 mm, with the small one in the center and big one at the edge to evenly distribute the gas pulse, which was then expanded into a 40 mm×2 mm×2 mm groove. The nozzle cap block was then outfitted with two stainless steel plates which form a 40 mm×0.04 mm slit. The slit was aligned parallel to the optical axis of the cavity and positioned to ensure the maximum overlap of the slit jet pulse with the infrared beam. This slit nozzle design provided a longer absorption path and a better spectral resolution compared to the previous slit nozzle design with a 15 mm×0.06 mm slit [4].

2.4 Rapid-scan and WMS methods

Our rapid scan scheme was similar to the original design of De Piante et al. [2] and the later ones by Howard et al. [24] and McKellar et al. [3]. To carry out such experiments with the CEA and the MPA spectrometers, two LabVIEW control program, i.e., *RapidScan* and *RapidOScope*, were developed. *RapidScan* facilitates the execution of the pulse sequences given in Fig. 3. For example, the DF-QCL was ramped continuously using a composed sawtooth wave (Fig. 3) generated using a function generator (Stanford Research Systems, DS345). The duration of each ramp is about

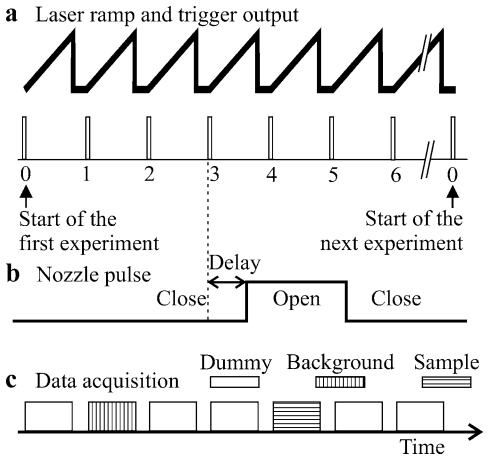

Fig. 3 The pulse sequence of the *RapidScan* program. See text for details

1.6 ms with a built-in 0.4 ms recovery period at the end of each ramp which helps to alleviate the frequency nonlinearity of the laser scan. To ramp the EC-QCL, a sine wave, instead of the sawtooth wave, at ∼100 Hz was used. The corresponding TTL triggers from the function generator were registered with the NI PCI-6251 multi-functional card. In a normal jet expansion experiment, a background signal was recorded at trigger number 1 (Fig. 3). The nozzle was then opened at trigger number 3 plus an adjustable delay time to insure the molecular jet expansion encompass the next laser scan starting at trigger number 4, in which a combined jet sample with background spectrum was recorded. The pure jet sample spectrum was then obtained by subtracting the background signal recorded from the signal with a molecular pulse. Both the nozzle delay time and the nozzle opening duration controlled by a valve driver (Iota ONE, Parker Hannifin) could be optimized experimentally to ensure the best temporal overlap of jet expansion with laser frequency scan.

RapidOScope was developed for even faster, real time data collection for either static gas sample or pseudo-cw-jet expansions using the same CEA and MPA spectrometer setups. A repetition rate, up to ∼1 kHz, was achieved. For the operation with pseudo-cw-jet expansions, the program rapidly collected tens to hundreds of laser scans which over-

lapped with a 20∼200 ms jet expansion pulse. It therefore allowed one to explore very different jet operation conditions.

A second detection scheme we implemented was the WMS method [25–35], which is a well known technique to improve the SNR of spectral measurements. It had recently been applied to CEA spectroscopy with QCLs [11, 13, 36]. For example, Vasudev [37] and Tittel et al. [11] had reported that WMS is a very effective way to remove the residual etalon fringes in the CEA spectra for static gas measurements, in addition to the off-axis coupling. To implement the WMS method in our experiments with the EC-QCL, the QCL frequency was scanned slowly with the laser PZT while a 10–200 kHz external sine modulation current was applied to the laser simultaneously through the input port of the laser driver. The signal from the MCT detector was fed into a lock-in amplifier (Stanford Research Systems, SR830) locked to the modulation frequency and the second order harmonic detection ($2f$ signal) was usually used. Besides the optimization of the usual parameters associated with WMS such as modulation frequency (Ω), laser frequency scan rate (ω), modulation depth, and time constant (τ), the transient nature of a jet expansion sample requires additional timing consideration. Two schemes, i.e., cw-jet [38–41] and fast-repetition step-scan [42–44], had been reported for the WMS detection of transient jet-cooled samples. We implemented both methods with the EC-QCL to measure the transitions of Ar–H_2O. The experimental details and the results with WMS are described in Sect. 4.

The infrared detector signal was digitized using a 14 bit, four channel analog-to-digital card (GageCompuScope 8340) with a 10 MS/s sample rate for each channel, and was then stored in a PC. The etalon fringes, reference gas spectrum, and jet expansion spectrum were recorded simultaneously. To convert the current scan into the frequency scale, the etalon fringes were fitted to a polynomial, typically second or third order for the DF-QCL, and the NH_3, N_2O and H_2O frequencies in HITRAN08 database [45] were used to determine the free spectral range of the etalon and the absolute frequencies. Because the EC-QCL was driven by a non-linear sine wave, in the frequency calibration procedure we fitted less than a quadrant of the laser scan cycle to a high order polynomial. The uncertainties in the transitions frequencies was typically within 0.001 cm^{-1} or better.

3 Results and discussions

In this section, we describe and discuss the static and jet-cooled spectra measured with the two QC lasers in combination with the CEA and MPA spectrometers. Because the DF-QCL operates in a very similar fashion as a lead salt diode laser whose combination with the MPA cell had been published before [4], only the new development of the DF-QCL with the CEA cell is presented in Sect. 3.1. In Sect. 3.2 the combination of the EC-QCL and the CEA cell using the rapid scan technique is described first. The difficulty in achieving a similar sensitivity as in Sect. 3.1 with the EC-QCL which has a much slower laser scan rate than the DF-QCL is discussed. In addition, attempts to use WMS technique to overcome this problem are also discussed. In Sect. 3.3, the combination of the EC-QCL with the MPA cell using the rapid scan technique is presented, as an alternative to overcome the disadvantage of the slow scan rate of the EC-QCL.

3.1 Spectra measured with the DF-QCL CEA spectrometer

In our early CEA experiments with the DF-QCL, one ring-down mirror was mounted on a mirror PZT (Polytec PI S-314.10) with a 10 mm clear aperture, which was used in the previous CRD experiments [5]. To increase the effective mirror size from 10 to 20 mm, a new mirror PZT (PiezoMechanik, HPSt 150/35-25/40TPVS45) was acquired. The new mirror PZT has a 25 mm diameter clear aperture and a maximum stroke of 40 μm. To maximize the surface usage of the existing 1″ ring-down mirrors, a homemade mirror mount with a clear aperture of 20 mm in diameter was used. In Fig. 4, we compare CEA measurements obtained with two different effective mirror surfaces, with the same experimental setup. With the 10 mm effective mirror size, the fringes due to the spurious laser build-ups inside the CEA cell were quite prominent, even after 1000 averaging cycles. With the 20 mm effective mirror size, such noise had the same order of magnitude as the detector noise. It was also noted that the laser power reached the MCT detector is much higher with the 10 mm effective mirror size than the 20 mm one, presumably because of the much higher mirror reflectivity at the center portions of the mirrors than at the edges. As a result, 20 torr of NH_3 was needed with the 10 mm mirror setup in order to observe the NH_3 transitions with a good SNR in Fig. 4(a) top trace, while only 2 mtorr of NH_3 was used to achieve the much better SNR with the 20 mm one (Fig. 4(a) bottom trace and Fig. 4(c)). It should be mentioned that since the spectrometers with a large vacuum chamber were designed to measure high resolution spectra of jet-cooled sample rather than for accurate quantitative static gas measurements, no special efforts were made to obtain highly accurate pressure measurements and use pre-calibrated static gas samples.

Another possible way to reduce spurious laser build-ups inside the CEA cell is to increase the laser scan rate (ω) so that there is not enough time at each frequency interval to get a significant laser power build-up, resulting in more evenly distributed mode intensities [46, 47]. On the other

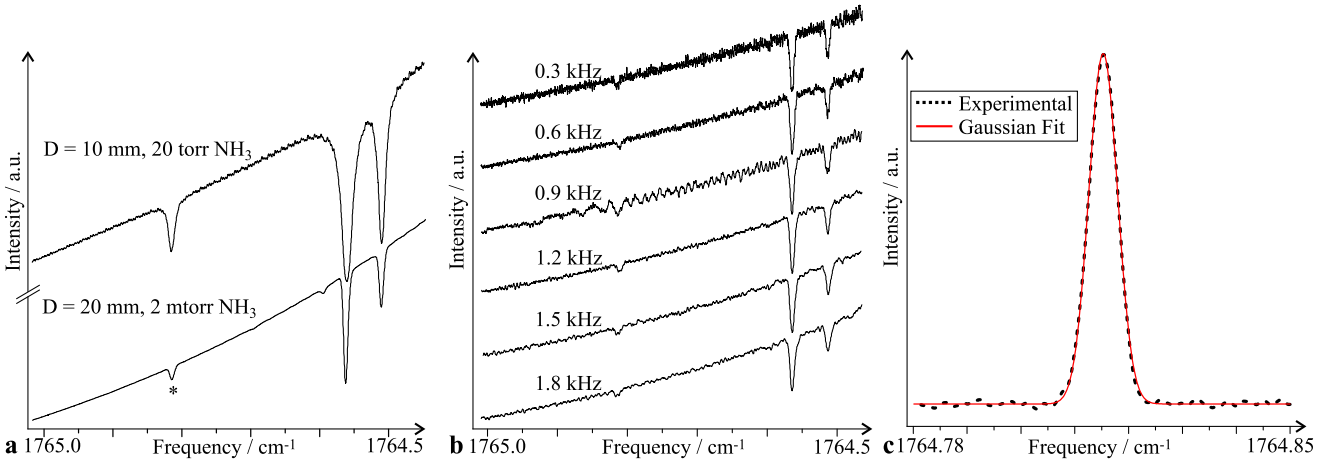

Fig. 4 (**a**) Upper trace was recorded with an effective mirror diameter of 10 mm and 20 torr of NH_3 in the CEA cavity; lower trace with an effective mirror diameter of 20 mm and 0.5% NH_3 in Ne with a total pressure of 400 mtorr. 1000 averaging cycles and a laser scan rate of 1.2 kHz were used for each spectrum. (**b**) The NH_3 spectra were recorded using six different laser scan rates ranging from 0.3 to 1.8 kHz, with a sample mixture of 0.5% NH_3 in Ne with a total pressure of 400 mtorr and one experimental cycle. (**c**) The NH_3 line at 1764.8155 cm^{-1}, indicated with * in (**a**), after baseline correction and frequency calibration. The *dotted curve* shows a Gaussian fit with a FWHM of $5.33\times10^{-3}cm^{-1}$. The signal-to-noise ratio, defined as $A/\delta A$, where A is the area under the absorption line and δA the deviation of A in the fit, is 653

hand, this also reduces the output laser power to the detector and may result in a lower SNR. It is therefore necessary to optimize laser scan rate experimentally. To illustrate the effects of varying laser scan rate, a small section of the NH_3 spectrum was recorded with the laser scan rates varying from 0.3 to 1.8 kHz. The baseline noise was considerably smaller with a scan rate of 1.2 kHz and higher. Not much further improvement was detected above 1.2 kHz since other noise sources such as detector noise also became important. Furthermore, the observed NH_3 transitions were broader at higher scan rates. Therefore, a laser scan rate of 0.7∼1.2 kHz was typically used in our experiments. Figure 4(c) shows the NH_3 line at 1764.81555 cm^{-1} recorded with 1000 averaging cycles, i.e., about 1 s data acquisition time. The experimental data points were fitted to a Gaussian profile. The experimental full width at half maximum (FWHM) was 5.33×10^{-3} cm^{-1}, slightly larger than the 5.27×10^{-3} cm^{-1} Doppler line width of NH_3 at 296 K. From the SNR achieved, the detection limit was calculated to be 1.77×10^{-8} cm^{-1}. This corresponds to a similar NH_3 detection limit reported previously [37].

To demonstrate the performance of the DF-QCL CEA spectrometer with a jet expansion for an organic molecule, we measured the infrared spectrum of the carbonyl stretching mode of methyl lactate, $CH_3OCOCH(OH)CH_3$. To obtain a jet-cooled spectrum, methyl lactate was placed in a bubbler with a water jacket kept at a temperature of 12°C. The argon carrier gas with a backing pressure of 200∼600 torr was forced through a molecular sieve inside the bubbler to ensure that the vapor of methyl lactate was efficiently mixed with Ar to be brought to the nozzle. The top of the infrared beam profile intercepted the molecular jet at about 1.0 cm below the nozzle slit. The repetition rate of the nozzle pulse was 5 Hz. Typical chamber pressures were less than 0.1 mtorr during the experiments. The rotational temperature achieved with such a jet expansion was estimated to be 2∼5 K [5]. Because of the very limited frequency coverage (1760.4–1766.0 cm^{-1}) provided by the DF-QCL, we could only access the region that is about 6 to 12 cm^{-1} away from the band origin (Fig. 5(a)) where the ro-vibrational transitions have diminishing intensities because of the low rotational temperature achieved. Indeed, no transition was observed except at the low end of the frequency region with the temperature of the QCL at its highest. An example jet-cooled spectrum of methyl lactate is given in Fig. 5(b), together with the etalon and the reference scans.

3.2 Spectra measured with the EC-QCL CEA spectrometer

The EC-QCL provides a much broader frequency coverage from 1592 to 1698 cm^{-1} than that of the DF-QCL. This allows us to carry out real molecular spectroscopic studies such as the investigation of the bending mode of water containing complexes like Ar–H_2O [48] and H_2–H_2O [49]. On the other hand, the fine tuning of the EC-QCL is driven by a laser PZT with the highest possible scan rate of only 100 Hz, which is much lower than the optimum rate of ∼1 kHz for CEA, as discussed in the previous section. Furthermore, the actual laser frequency scan is not linear since the laser PZT is designed to be driven by a sine wave. Although with the current modulation to the EC-QCL one can scan a spectral range up to 0.1 cm^{-1} at 10 kHz∼2 MHz, it is not an

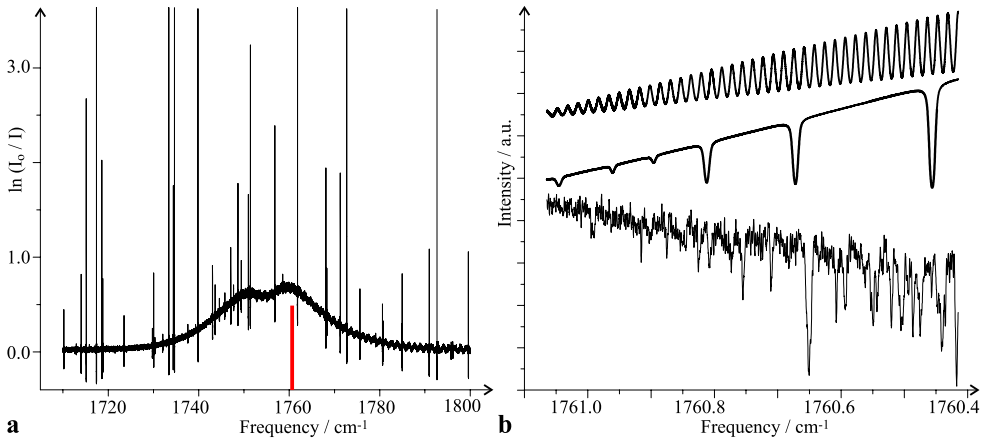

Fig. 5 (**a**) A room temperature static gas spectrum of methyl lactate in the frequency region from 1710 to 1800 cm^{-1}. The *strong sharp lines* are due to water vapor. The targeted frequency region for the laser experiments is indicated with a *red stick*. (**b**) A calibrated jet-cooled ro-vibrational spectrum of methyl lactate, together with the etalon and the reference scans where the known NH_3 and H_2O frequencies were fitted with a standard deviation of 0.0008 cm^{-1}

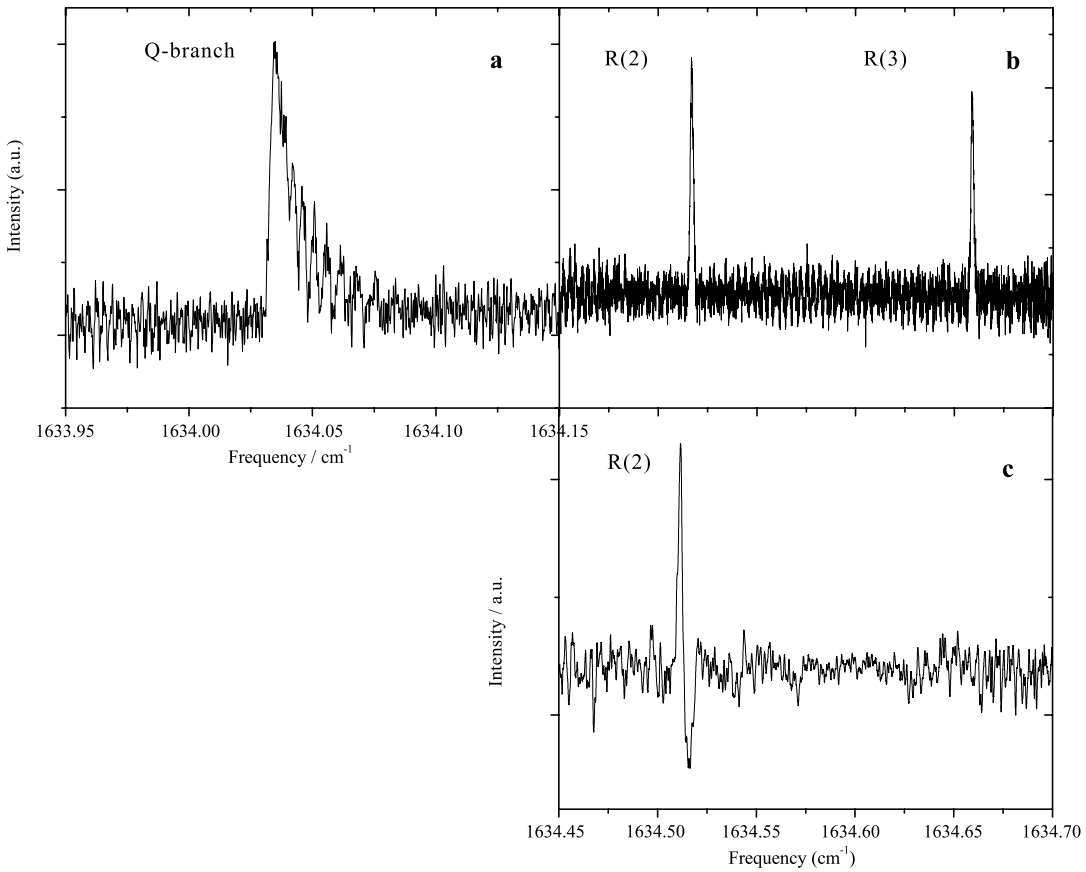

Fig. 6 Example spectra of the $\Pi(1_{11}) \leftarrow \Sigma(0_{00})$ band of Ar–*para* H_2O recorded with 1000 averaging cycles with the EC-QCL CEA spectrometer: (**a**) rapid scan spectrum of the Q-branch, (**b**) rapid scan spectrum of the R-branch, (**c**) the WMS spectrum of the R(2) transition. The sample mixture contains 0.4% water and 6% Ar in 5000 torr Ne. The rapid scan spectra were measured with 100 Hz laser scan rate and 3 ms nozzle opening duration. The WMS spectrum was measured with 1 Hz laser scan rate and 30 ms nozzle opening duration, with $\Omega = 50$ kHz and 0.3 ms time constant for the lock-in amplifier. See text for details

applicable method for molecular spectroscopic applications because it is very difficult to perform frequency calibration for such a narrow spectral range and line width broadening was observed at high laser scan frequency. This approach was therefore not further pursued. Figure 6 shows two examples spectra of the Ar–*para* H_2O $\Pi(1_{11}) \leftarrow \Sigma(0_{00})$ band recorded with the CEA spectrometer. Because of the many averaging cycles needed, the spectral line width was broadened to 0.002 cm^{-1}, which is twice as large as that in a 1-shot jet-cooled spectrum with the MPA spectrometer (vide

infra). Based on the optical depth obtained from the static gas measurement, the effective absorption path of the CEA configuration was estimated to be ∼400 m, which was about twice as long as that obtained with the MPA spectrometer. However, the sensitivity achieved is only modest compared with the MPA configuration because of the low laser PZT scan rate (vide infra). The dominant noise came from incomplete averaging of the cavity transmission resonances because of the low laser scan rate with the EC-QCL.

In an attempt to achieve a better sensitivity, we implemented both cw-jet and fast-repetition step-scan method for the WMS detection of the jet signal. Since the maximum pulse-to-pulse repetition rate for our experiments is ∼1 Hz, the EC-QCL had to be scanned (with laser PZT rate) extremely slow to obtain decent spectral resolution in the fast-repetition step-scan method. For example, a jet-cooled transition with 0.002 cm^{-1} line width would require that 1 cm^{-1} spectral range was scanned in no shorter than 2500 s to ensure at least 5 data points were collected to plot this transition. Such low laser scan rate leads to poor laser frequency stability and large $1/f$ noise. Moreover, the pulse-to-pulse sample fluctuation was the dominant noise source in the observed spectra and such fluctuation could be very large (10∼30%) with the general valve nozzle. Overall, this method was time and sample consuming and unsatisfactory for the jet experiments.

It is impossible to perform cw-jet experiments with the current pumping system. Instead, we used the pseudo-cw-jet WMS approach where the slit nozzle was opened for a long enough time period to allow harmonic detection of the jet signal within one pulse. To carry out such pseudo-cw-jet WMS experiments, we first optimized several WMS parameters using Q(10) transition of the 0001–0110 band of N_2O. The effects of these parameters on the SNR of the transition are summarized in Fig. 7. For pseudo-cw-jet experiment, we observed that the existence of jet-cooled sample could last for as long as 10 ms. During such time period a spectrum of 0.2∼0.02 cm^{-1} could be obtained with a 10∼1 Hz laser frequency scan rate. The whole measurement process was finished within a single long-pulsed jet. An example $2f$ spectrum obtained for R(2) transition of Ar–*para* H_2O is given in Fig. 6(c). The line shape looks distorted on the low frequency side because the pulsed jet finished at this frequency already, or in other words, one would have to leave the jet on longer to cover the rest of the frequency region. The SNR obtained with this method was much better than that with the step-scan scheme and similar to that with rapid scan method in one experimental cycle. One noticeable drawback, however, is the limited spectral coverage obtained during each jet pulse. For example, only R(2) appears in Fig. 6(c), while R(3) is not there because of the sample pulse does not last long enough for the R(3) transition to be measured. Therefore, to cover a 1 cm^{-1} spectral range, one needs to piece together several narrow spectral sections. This makes it tedious and difficult to perform frequency calibration and spectral searches.

3.3 Spectra measured with the EC-QCL MPA spectrometer

It is our experience that the regular multi-pass setup is considerably less sensitive to the laser frequency scan rate in the range of 100 Hz to a few kHz than the CEA setup. Therefore, we also evaluated the performance of the EC-QCL coupled with the MPA spectrometer by measuring the static N_2O and jet-cooled Ar–H_2O spectra. The spectra of the N_2O Q(9) and Q(8) transitions measured with different laser frequency scan rates, multi-pass configurations, and sample pressures are summarized in Fig. 8. As one can see, the SNR increases as the laser frequency scan rate is increased since there is less background noise ($1/f$) at higher frequency and the absorption coefficient varies linearly with the sample pressure and the number of optical passes. As can also be observed from the residual of the Voigt fit, the recorded line shape is asymmetric, most likely due to the rapid passage effect [50, 51].

A typical jet-cooled spectrum of Ar–*para* H_2O recorded is depicted in Fig. 9. Though the spectrum was obtained with only one experimental cycle, the SNR obtained was already better than the previous reported one with a lead salt diode laser [48] because of the higher QCL power and a much longer absorption path. The SNR achieved is also clearly superior compared to that with the CEA spectrometer. Such superiority was also reported by Menzel et al. [9], where a MPA spectrometer with a 100 m absorption path gave a detection limit 100 times lower than that achieved with an on-axis CEA configuration with an effective absorption path of 670 m.

In Fig. 10, we compare the 1-cycle and 50-cycle spectra of the R(1) transition of Ar–*para* H_2O. The slightly distorted line shape is due to the rapid passage effects [50, 51]. The observed transitions were fitted to a Gaussian line shape and the line width (FWHM) for the 1-cycle and 50-cycle peaks were 0.0013 and 0.0022 cm^{-1}, i.e., 40 and 65 MHz, respectively. This highlights the challenges associated with the measurement of jet-cooled spectra. Since the desirable line width is very narrow, even a small laser jitter from one scan to the next results in noticeable line width broadening. From the close-up spectra in Fig. 10 one can also see that the dominant noises sources are the interference fringes generated by the optical components and the multi-pass cell which cannot be satisfactorily depressed by averaging more cycles. Thus the SNR does not improve linearly with the square root of a even small number of cycles.

Overall, the combination of the QCL with the astigmatic multi-pass cell is a highly desirable one because the high

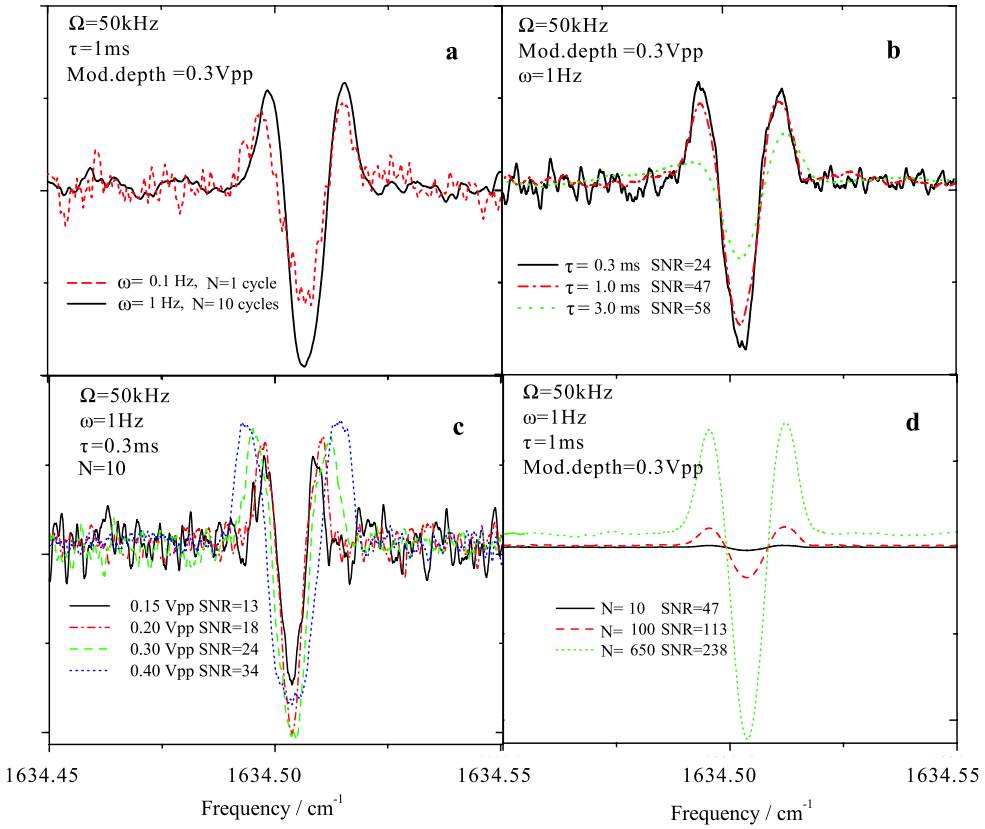

Fig. 7 WMS spectra of N_2O Q(10) line measured with different laser PZT rate (ω), lock-in amplifier time constant (τ), modulation depth, and average cycles (N): (**a**) Comparison of the spectra obtained with a laser PZT rate of 1 Hz and 10 cycles with a laser PZT rate of 0.1 Hz and 1 cycle. This shows that with the same data acquisition time the first gives a much better SNR; (**b**) The effects of the lock-in amplifier time constant. The typical value used was 0.3 or 1.0 ms without severe distortion of the line shape; (**c**) The effects of the modulation depth on the SNR and line width. Noticeable line broadening was observed as the modulation depth increase to 0.4 Vpp. A typical value used for jet experiments is 0.15 Vpp. (**d**) The relationship between the average cycles and the SNR deviates slightly from the $\sqrt{N}$ rule when N reaches several hundred

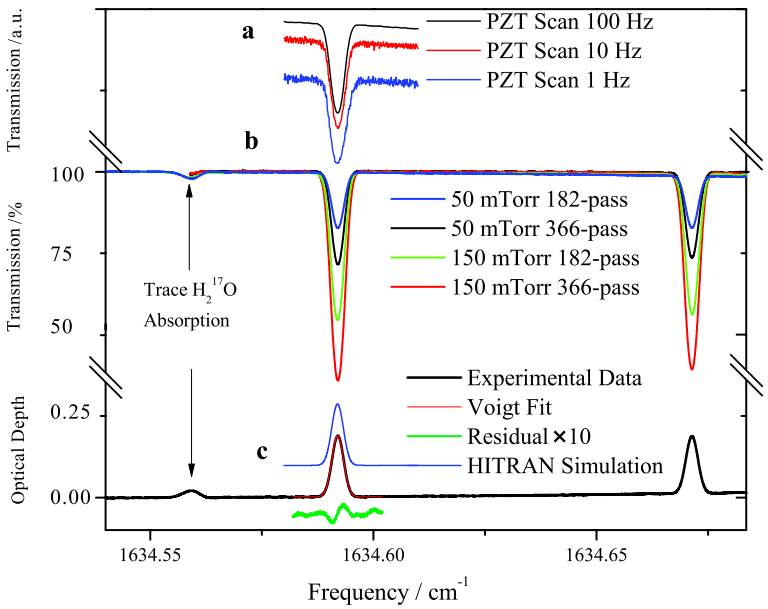

Fig. 8 Transmission spectra of $(\frac{I}{I_0})$ of 50 or 150 mtorr N_2O with different absorption path: (**a**) One cycle scan of the N_2O Q(9) transition with the laser frequency scan rate at 100, 10, and 1 Hz, i.e., ~0.1, 0.01, and 0.001 cm^{-1}/ms; (**b**) 100 cycle average of 50 or 150 mtorr N_2O Q(9) and Q(8) transitions with the 182-pass or 366-pass alignment pattern; (**c**) The experimental, HITRAN simulation, and Voigt fit of the optical depth of the Q(9) transition measured with 50 mtorr sample pressure and 182-pass pattern

QCL power permits the usage of the very long absorption path affordable by the astigmatic pattern while remaining adequate to the detector. For the molecular spectroscopic measurement of a jet-cooled sample, the combination of the EC-QCL with the MPA spectrometer is the most suitable choice, as demonstrated here.

4 Conclusion

The design and construction of two QCL based off-axis CEA and MPA spectrometers have been reported. Their performance has been evaluated by recording several infrared spectra of both static gas and jet-cooled samples. With the

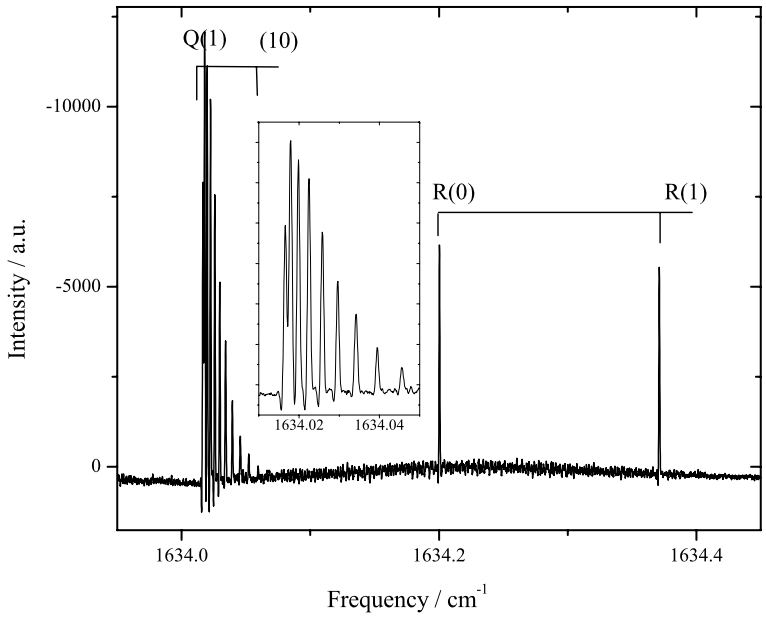

Fig. 9 Rapid scan spectrum of Ar–*para* H_2O measured with one experimental cycle and 366-pass MPA pattern. The laser PZT rate is 100 Hz. The transitions and sample mixture used are the same as in Fig. 6

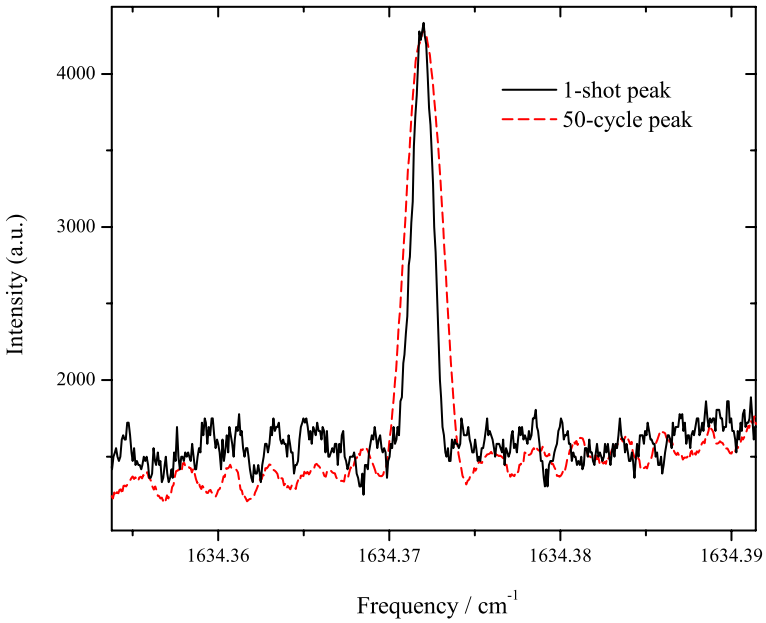

Fig. 10 R(1) transition of Ar–*para* H_2O $\Pi(1_{11}) \leftarrow \Sigma(0_{00})$ band recorded with 1 cycle and 50 cycles. For this particular transition, we had reduced the laser power used to minimize the asymmetry in the line shape so that one can easily observe the line broadening effect due to averaging

DF-QCL, the detection limit obtained was 1.8×10^{-8} cm^{-1} for the CEA spectrometer with an optimal laser frequency scan rate of ~1 kHz. The detection limit achieved was considerably worse with the EC-QCL because of the low scan rate (<100 Hz) possible. The WMS method has been applied in order to improve the detection sensitivity of the EC-QCL CEA spectrometer although with only moderate success. Further improvement in detection limit can be expected with usage of larger ring-down mirrors such as those with a diameter of 2″. Compared to the DF-QCL, the EC-QCL is well suited for the high resolution molecular spectroscopic measurement with its wide frequency coverage and cw MHF tuning capability. The combination of the MPA spectrometer with the EC-QCL has been identified as the best choice for high resolution spectroscopic studies of jet-cooled samples among the configurations evaluated here. Excellent SNR has been demonstrated for the infrared spectra of the Ar–*para* H_2O complex with this combination.

Acknowledgements This research was funded by the University of Alberta, the Natural Sciences and Engineering Research Council (NSERC) of Canada, the Canada Foundation for Innovation, Alberta Ingenuity and Petro-Canada. We thank Dr. A.R.W. McKellar at Steacie Institute for Molecular Sciences, National Research Council of Canada for the survey spectrum of methyl lactate. We also thank Dr. Y.A. Bakhirkin of Rice University for generously sharing his expertise with liquid nitrogen cooled quantum cascade lasers, Dr. N. Moazzen-Ahmadi and L. Murdock for sharing their experience in designing

heaters for mirrors, and Drs. W. Jäger, P. Raston, and O. Sukhorukov for discussions. Z.S. and X.L. thank Alberta Ingenuity for Studentships.

References

1. G. Springholz, T. Schwarzl, W. Heiss, A. Krier, *Mid-infrared Semiconductor Optoelectronics* (Springer, London, 2006)
2. A. De Piante, E.J. Campbell, S.J. Buelow, Rev. Sci. Instrum. **60**, 858 (1989)
3. M.D. Brookes, C. Xia, J. Tang, J.A. Anstey, B.G. Fulsom, K.X. Au Yong, J.M. King, A.R.W. McKellar, Spectrochim. Acta Part A **60**, 3235 (2004)
4. Z. Su, W.S. Tam, Y. Xu, J. Chem. Phys. **124**, 024311 (2006)
5. W.S. Tam, I. Leonov, Y. Xu, Rev. Sci. Instrum. **77**, 063117 (2006)
6. J. Faist, C. Gmachl, F. Capasso, C. Sirtori, D.L. Sivco, J.N. Baillargeon, A.Y. Cho, Science **264**, 553 (1994)
7. D. Hofstetter, J. Faist, I.T. Sorokina, K.L. Vodopyanov, *Solid-State Mid-Infrared Laser Sources* (Springer, Berlin, 2003)
8. M. Beck, D. Hofstetter, T. Aellen, J. Faist, U. Oesterle, M. Ilegems, E. Gini, H. Melchior, Science **295**, 301 (2002)
9. L. Menzel, A.A. Kosterev, R.F. Curl, F.K. Tittel, C. Gmachl, F. Capasso, D.L. Sivco, J.N. Baillargeon, A.L. Hutchinson, A.Y. Cho, W. Urban, Appl. Phys. B **72**, 859 (2001)
10. A.A. Kosterev, A.L. Malinovsky, F.K. Tittel, C. Gmachl, F. Capasso, D.L. Sivco, J.N. Baillargeon, A.L. Hutchinson, A.Y. Cho, Appl. Opt. **40**, 5522 (2001)
11. Y.A. Bakhirkin, A.A. Kosterev, C. Roller, R.F. Curl, F.K. Tittel, Appl. Opt. **43**, 2257 (2004)
12. G. Wysocki, R.F. Curl, F.K. Tittel, R. Maulini, J.M. Bulliard, J. Faist, Appl. Phys. B **81**, 769 (2005)
13. Y.A. Bakhirkin, A.A. Kosterev, R.F. Curl, F.K. Tittel, D.A. Yarekha, L. Hvozdara, M. Giovannini, J. Faist, Appl. Phys. B **82**, 149 (2006)
14. M.R. McCurdy, Y.A. Bakhirkin, F.K. Tittel, Appl. Phys. B **85**, 445 (2006)
15. M.R. McCurdy, Y. Bakhirkin, G. Wysocki, F.K. Tittel, J. Biomed. Opt. **12**, 034034 (2007)
16. A. Kosterev, G. Wysocki, Y. Bakhirkin, S. So, R. Lewicki, M. Fraser, F. Tittel, R.F. Cur, Appl. Phys. B **90**, 165 (2008)
17. F.K. Tittel, G. Wysocki, A. Kosterev, Y. Bakhirkin, *Mid-Infrared Coherent Sources and Applications* (Springerr, Dordrecht, 2008)
18. T. Day, M. Weida, D. Arnone, M. Pushkarsky, M.A. Druy, C.D. Brown, R.A. Crocombe, *Next-Generation Spectroscopic Technologies II*, vol. 7319 (SPIE, Orlando, 2009), 73190F–7
19. T. Day, E.B. Takeuchi, M. Weida, D. Arnone, M. Pushkarsky, D. Boyden, D. Caffey, M. Dubinskii, S.G. Post, *Laser Technology for Defense, Security V*, vol. 7325 (SPIE, Orlando, 2009), 73250J–6
20. D. Herriott, H. Kogelnik, R. Kompfner, Appl. Opt. **3**, 523 (1964)
21. G.S. Engle, W.S. Drisdell, F.N. Keutsch, E.J. Moyer, J.G. Anderson, Appl. Opt. **45**, 9221 (2006)
22. J.B. McManus, P.L. Kebabian, M.S. Zahniser, Appl. Opt. **34**, 3336 (1995)
23. P. Birza, T. Motylewski, D. Khoroshev, A. Chirokolava, H. Linnartz, J.P. Maier, Chem. Phys. **283**, 119 (2002)
24. G.D. Hayman, J. Hodge, B.J. Howard, J.S. Muenter, T.R. Dyke, Chem. Phys. Lett. **118**, 12 (1985)
25. G.C. Bjorklund, Opt. Lett. **5**, 15 (1980)
26. D.E. Cooper, T.F. Gallagher, Appl. Opt. **24**, 1327 (1985)
27. M. Gehrtz, G.C. Bjorklund, E.A. Whittaker, J. Opt. Soc. Am. B **2**, 1510 (1985)
28. J.A. Silver, Appl. Opt. **31**, 707 (1992)
29. J.M. Supplee, E.A. Whittaker, W. Lenth, Appl. Opt. **33**, 6294 (1994)
30. K. Shahnazi, Appl. Opt. **37**, 2502 (1998)
31. G.E. Hall, S.W. North, Annu. Rev. Phys. Chem. **51**, 243 (2000)
32. C.A. Taatjes, J.F. Hershberger, Annu. Rev. Phys. Chem. **52**, 41 (2001)
33. J. Ye, J.L. Hall, Phys. Rev. A **61**, 061802 (2000)
34. J. Ye, L. Ma, J.L. Hall, Opt. Lett. **21**, 1000 (1996)
35. G. Friedrichs, Z. Phys. Chem. **222**, 1 (2008)
36. A. Zybin, Y.A. Kuritsyn, V.R. Mironenko, K. Niemax, Appl. Phys. B **78**, 103 (2004)
37. R. Vasudev, Appl. Phys. B **87**, 163 (2007)
38. Z. Wang, M. Eliades, K. Carron, J.W. Bevan, Rev. Sci. Instrum. **62**, 21 (1991)
39. Y. Xu, A.R.W. McKellar, J. Chem. Phys. **104**, 2488 (1996)
40. Y. Xu, S. Civiš, A.R.W. McKellar, Mol. Phys. **87**, 1071 (1996)
41. Y. Xu, A.R.W. McKellar, Mol. Phys. **88**, 859 (1996)
42. S. Davis, M. Fárník, D. Uy, D.J. Nesbitt, Chem. Phys. Lett. **344**, 23 (2001)
43. M. Havenith, G. Hilpert, M. Petri, W. Urban, Mol. Phys. **81**, 1003 (1994)
44. I. Pak, M. Hepp, D.A. Roth, G. Winnewisser, Rev. Sci. Instrum. **68**, 1668 (1997)
45. L.S. Rothman, I.E. Gordon, A. Barbe, D. Chris Benner, P.F. Bernath, M. Birk, V. Boudon, L.R. Brown, A. Campargue, J.-P. Champion, K. Chance, L.H. Coudert, V. Dana, V.M. Devi, S. Fally, J.-M. Flaud, R.R. Gamache, A. Goldman, D. Jacquemart, I. Kleiner, N. Lacome, W.J. Lafferty, J.-Y. Mandin, S.T. Massie, S.N. Mikhailenko, C.E. Miller, N. Moazzen-Ahmadi, O.V. Naumenko, A.V. Nikitin, J. Orphal, V.I. Perevalov, A. Perrin, A. Predoi-Cross, C.P. Rinsland, M. Rotger, M. Šimečková, M.A.H. Smith, K. Sung, S.A. Tashkun, J. Tennyson, R.A. Toth, A.C. Vandaele, J. Vander Auwera, J. Quant. Spectrosc. Radiat. Transfer **110**, 533 (2009)
46. G. Berden, R. Peeters, G. Meijer, Int. Rev. Phys. Chem. **19**, 565 (2000)
47. B. Bakowski, L. Corner, G. Hancock, R. Kotchie, R. Peverall, G.A.D. Ritchie, Appl. Phys. B **75**, 745 (2002)
48. M.J. Weida, D.J. Nesbitt, J. Chem. Phys. **106**, 3078 (1997)
49. M.J. Weida, D.J. Nesbitt, J. Chem. Phys. **110**, 156 (1999)
50. G. Duxbury, N. Langford, M.T. McCulloch, S. Wright, Chem. Soc. Rev. **34**, 921 (2005)
51. M.T. McCulloch, G. Duxbury, N. Langford, Mol. Phys. **104**, 2767 (2009)